Inorganic Chemistry

Article

pubs.acs.org/IC

Syntheses, Structures, and Properties of New Manganese Carbonyls as Photoactive CO-Releasing Molecules: Design Strategies That Lead to CO Photolability in the Visible Region

Margarita A. Gonzalez, Samantha J. Carrington, Nicole L. Fry, Jose L. Martinez, and Pradip K. Mascharak*

Department of Chemistry and Biochemistry, University of California, Santa Cruz, California 95064, United States

Supporting Information

ABSTRACT: The unusual role of CO as a signaling molecule in several physiological pathways has spurred research in the area of synthesizing new CO-releasing molecules (CORMs) as exogenous CO donors. Auxiliary control on CO delivery can be achieved if CO can be released under the control of light. To synthesize such photoactive CORMs (photoCORMs) with the aid of smart design, a series of manganese carbonyls have been synthesized with ligands that contain extended conjugation and electron-rich donors on their frames. Five such photoCORMs, namely, $[Mn(pimq)(CO)_3(MeCN)]ClO_4$ (**1**, where pimq = (2-phenyliminomethyl)quinoline), $[Mn(qmtpm)(CO)_3(MeCN)]ClO_4$ (**2**, where qmtpm = 2-quinoline-*N*-(2′-methylthiophenyl) methyleneimine), $[Mn(qmtpm)(CO)_3Br]$ (**3**) $[Mn(pmtpm)(CO)_3(MeCN)]ClO_4$ (**4**, where pmtpm = 2-pyridyl-*N*-(2′-methylthiophenyl)methyleneimine), and $[Mn(pmtpm)(CO)_3Br]$ (**5**), have been synthesized and structurally characterized. These designed carbonyls readily release CO upon exposure to light (400−550 nm). The apparent CO release rates and quantum yield values at 509 nm (ϕ_{509}) of the photoCORMs increase steadily with rise in conjugation in the ligand frame and inclusion of a −SMe group. Addition of Br^- as an ancillary ligand also improves the CO-donating capacity. Results of density functional theory (DFT) and time dependent DFT (TDDFT) studies indicate that low energy metal-to-ligand charge transfer (MLCT) transitions from Mn-CO bonding into ligand-π orbitals lead to reduction of M-CO(π^*) back-bonding and loss of CO from these photoCORMs. Inclusion of −SMe and Br^- in the coordination sphere attenuates the energies of the HOMO and LUMO levels and causes further enhancement of CO photorelease. Collectively, the results of this work demonstrate that new photoCORMs with excellent sensitivity to visible light can be synthesized on the basis of smart design principles.

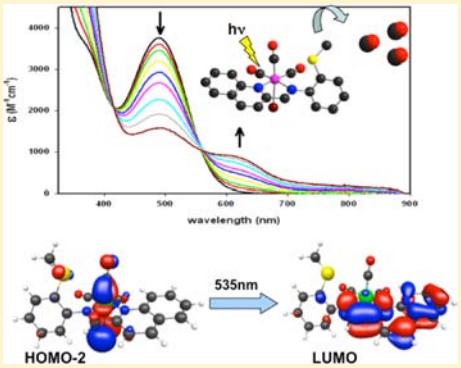

INTRODUCTION

Carbon monoxide (CO), the once obscure byproduct of heme catabolism by heme oxygenase (HO), has recently been the subject of intense scrutiny for its pertinent role in several physiological pathways.[1] Although substrates of CO may not be as diverse as that of another endogenously produced molecule nitric oxide (NO), CO has been known to mediate in key processes including vasorelaxation,[2] cell signaling,[3] and antiapoptotic activity.[4] In most cases, CO interacts with heme-containing metalloproteins. For instance, CO-induced vasodilation proceeds through binding to soluble guanylate cyclase (sGC) and to heme groups within the network of large conductance Ca^{2+}-activated potassium channels (BK_{Ca}).[2] A number of CO-dependent signaling processes include interaction of CO with mitochondrial cytochromes[5] and mitogen activated protein kinases (MAPK).[6] It is within these signaling cascades that CO imparts its protective action and establishes itself as a potent cytoprotective agent. Elevated CO levels concomitant with the induction of the stress protein HO have been associated with the attenuation of ischemia/reperfusion injury,[7] aid of organ graft survival,[8] and modulation of inflammatory conditions such as lung injury[9] and myocardial infarction.[10]

The salutary effects of endogenously produced CO have spurred efforts toward the preparation of exogenous CO donors to serve as novel therapeutics, as direct application of CO gas is often quite difficult. During the past few years, the CO complexes of low valent transition metals (metal carbonyls) have drawn attention as carbon monoxide releasing molecules (CORMs) that could serve as CO donors to biological targets.[11] Motterlini and co-workers synthesized the first in a series of water-soluble CORMs, $[Ru(glycinate)(CO)_3Cl]$ (often referred to as CORM-3),[12] by incorporating a glycine moiety to a typical Ru starting salt. Similar strategies were performed in the isolation of amino acid and amino ester-modified CORMs from group 6 metal centers.[13] These CORMs release CO upon dissolution to aqueous media. Solvent-assisted CO release was also achieved with the use of biocompatible pyrone groups and cyanocobalamin scaffolds in Fe/Mo[14] and Re-based[15] CORMs, respectively. Variation of ancillary ligands in the case of tetrachlorocarbonyliridates has resulted in a modulation of CO donation in aqueous media.[16] Our initial work on Fe-based CORMs derived from designed

Received: August 20, 2012
Published: October 22, 2012

dx.doi.org/10.1021/ic3018216 | *Inorg. Chem.* 2012, 51, 11930−11940

polypyridyl ligands have demonstrated the effect of trans ligands on the rates of CO release, as well as the role of K^+-channels in CO-induced vasodilation.[17] Although solvent-assisted CO release may be a desirable property in some cases, more control on initiating CO donation is necessary to achieve managed delivery of this potentially toxic gas.

Metal carbonyls have been known to release CO through photodissociation. The prototypical CORMs employed in previous biological assays were commercially available homoleptic metal carbonyls such as $[Mn_2(CO)_{10}]$[18] and $[Fe(CO)_5]$[19] which released CO upon laser flash photolysis. Ford and co-workers reported the photochemical reaction of a water-soluble salt $Na_3[W(CO)_5(TPPTS)]$ under UV irradiation and dubbed the term "photoCORM" to describe this type of light-triggered CO releasing compounds.[20] The iron carbonyl $[Fe(CO)(N4Py)](ClO_4)_2$, derived from a polypyridine ligand, also exhibits fast CO delivery upon illumination with UV light.[21] Sulfur-based ligands such as cysteamine and dithiocarbamate derivatives have recently been employed in the syntheses of photoactive Fe[22] and water-soluble Mn[23] photoCORMs, respectively.

Initial success in isolating photoCORMs has prompted research in exploring design principles that could provide ligands suitable for generating photosensitive metal carbonyls as suitable CO-delivery agents. Recently, a few manganese(I) tricarbonyl complexes derived from the tripodal ligands tris(pyrazolyl)methane and tris(imidazolyl)phosphane have been investigated by Schatzschneider and co-workers.[24] These photoCORMs release CO upon exposure to UV light much like $Na_3[W(CO)_5(TPPTS)]$ and $[Fe(CO)(N4Py)](ClO_4)_2$. We have utilized a series of tridentate polypyridine ligands with varying degree of conjugation to better understand the design principles that promote CO release from the subset of photoCORMs of the composition *fac*-$[Mn^I(L)(CO)_3]$ (L = tridentate ligands).[25] We discovered that increased conjugation in the ligand frame results in a systematic increase in absorptivity of the corresponding compounds in the longer wavelength region, thus generating photoCORMs more sensitive to light in the more desirable visible range. The carbonyl $[Mn(pqa)(CO)_3]ClO_4$ (where pqa = (2-pyridylmethyl)(2-quinolylmethyl)amine) which features both a pyridine and quinoline moiety (Figure 1), exhibits a strong

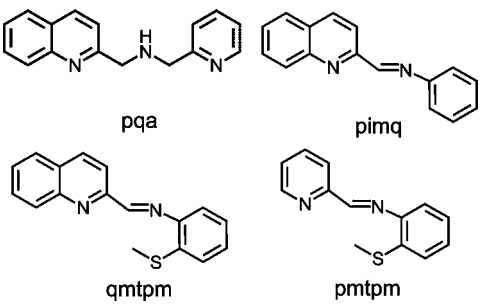

Figure 1. Structures of the ligands.

absorption band with λ_{max} at 360 nm. This is a notable red-shift in the absorption maximum when compared to the related carbonyl $[Mn(tpa)(CO)_3]ClO_4$ (where tpa = tri(2-pyridyl)-amine, λ_{max} = 330 nm) which comprises only pyridine donors in the otherwise similar ligand frame. Since the affinity of CO toward metals in low oxidation state arises predominantly from backbonding of electrons from the metal center to the π^* level of CO, we hypothesized that metal-to-ligand charge transfer (MLCT) transitions would reduce CO affinity of the metal center and result in CO photorelease. Indeed, increased CO photolability of $[Mn(pqa)(CO)_3]ClO_4$ compared to $[Mn(tpa)(CO)_3]ClO_4$ indicates that facilitation of CO photorelease could arise from such transition(s).

To explore the validity of our hypothesis further, we have now designed a series of manganese(I) carbonyls featuring bidentate and potentially tridentate ligands that incorporate both conjugated aromatic nitrogen donors and an imine functionality (in place of the amine nitrogen) in the ligand framework. To probe the effects of ancillary ligands, a Br^- ligand has also been incorporated in the coordination sphere. Finally, a thioether moiety has been added to the ligand frame to compete for a coordination site and promote additional CO release. The structures of the ligands employed in the present work are shown in Figure 1. We herein report the syntheses, structures, and photochemical parameters of $[Mn(pimq)(CO)_3(MeCN)]ClO_4$ (**1**, where pimq = (2-phenyliminomethyl)quinoline), $[Mn(qmtpm)(CO)_3(MeCN)]ClO_4$ (**2**, where qmtpm =2-quinoline-*N*-(2′-methylthiophenyl) methyleneimine), $[Mn(qmtpm)(CO)_3Br]$ (**3**) $[Mn(pmtpm)(CO)_3(MeCN)]ClO_4$ (**4**, where pmtpm =2-pyridyl-*N*-(2′-methylthiophenyl)methyleneimine), and $[Mn(pmtpm)(CO)_3Br]$ (**5**). The systematic changes in the ligand frame has afforded progressive red shift of the absorption band maximum from 390 nm (for **4**) to 535 nm (for **3**) in this set of photoCORMs. We have also attempted to correlate the CO photolability of these photoCORMs with the results of density functional theory (DFT) and time dependent DFT (TDDFT) calculations and confirm the nature of the MLCT associated with CO release.

EXPERIMENTAL SECTION

General Procedures. All experimental manipulations were performed under anaerobic conditions using standard Schlenk techniques and under limited light conditions. Manganese pentacarbonyl bromide ($[Mn(CO)_5Br]$) was purchased from Alfa Aesar. The ligands 2-pyridyl-*N*-(2′-methylthiophenyl)methyleneimine (pmtpm)[26] and 2-quinoline-*N*-(2′-methylthiophenyl) methyleneimine (qmtpm)[27] and the starting salt, *fac*-$[Mn(CO)_3(MeCN)_3](ClO_4)$[28] were synthesized following published procedures. Solvents were purified and/or dried by standard techniques prior to use.

Caution! *Transition metal perchlorates should be prepared in small quantities and handled with great caution as metal perchlorates may explode upon heating.*

2-(Phenyliminomethyl)quinoline (pimq). The synthesis and purification of pimq were modified to some extent compared to the procedure reported by Hamer.[29] Aniline (0.80 g, 8.60 mmol) was dissolved in 15 mL of MeOH followed by the addition of quinoline-2-carboxaldehyde (1.23 g, 7.81 mmol) in 15 mL of MeOH. The mixture was heated to reflux for 12 h, after which the solvent was removed under reduced pressure to obtain an orange-red oil. Upon addition of 30 mL of Et_2O and rapid scratching, the product separated as an orange powder. The solid was filtered and dried in vacuo (0.69 g, 60% yield). ^1H NMR (CD_3CN, 500 MHz), δ (ppm from TMS): 8.74 (s, 1H), 8.37 (d, 1H), 8.30 (d, 1H), 8.12 (d, 1H), 7.98 (d, 1H), 7.80 (t, 1H), 7.66 (t, 1H), 7.47 (t, 2H), 7.38 (d, 2H), 7.33 (t, 1H).

$[Mn(pimq)(CO)_3(MeCN)]ClO_4$ (1). A batch of $[Mn(CO)_3(MeCN)_3]ClO_4$ (0.378 g, 0.97 mmol) was added to a degassed solution of pimq (0.225 g, 0.97 mmol) in 25 mL of $CHCl_3$. The clear yellow orange color of the solution deepened to red brown upon reflux under N_2 atmosphere. After 6 h, the solvent was removed under reduced pressure, and the residue was triturated three times with Et_2O to obtain a red orange powder (0.364 g, 90% yield). Slow diffusion of pentane into a dichloromethane solution of **1** afforded red blade-like

dx.doi.org/10.1021/ic3018216 | *Inorg. Chem.* 2012, 51, 11930−11940

Table 1. Summary of Crystal Data, Intensity Collection, and Refinement Parameters for $[Mn(pimq)(CO)_3(MeCN)]ClO_4$ (1), $[Mn(qmtpm)(CO)_3(MeCN)]ClO_4$ (2), $[Mn(qmtpm)(CO)_3Br]$ (3), $[Mn(pmtpm)(CO)_3(MeCN)]ClO_4$ (4), and $[Mn(pmtpm)(CO)_3Br]$ (5)

	1	2	3	4	5
empirical formula	$C_{21}H_{15}ClMnN_3O_7$	$C_{22}H_{17}ClMnN_3O_7S$	$C_{20}H_{14}BrMnN_2O_3S$	$C_{18}H_{12}ClMnN_3O_7S$	$C_{16}H_{12}BrMnN_2O_3S$
FW.	511.75	557.85	497.24	504.77	447.19
cryst color	red blades	red orange blades	red blades	orange blades	red blades
T	296(2)	298(2)	296(2)	296(2)	296(2)
cryst syst	monoclinic	monoclinic	monoclinic	triclinic	triclinic
space grp	$C2/c$	$C2/c$	$P2(1)/n$	$P\bar{1}$	$P\bar{1}$
a (Å)	17.3321(6)	31.8928(8)	10.0170(8)	8.8047(6)	7.7145(6)
b (Å)	22.4429(8)	14.0999(4)	11.5945(10)	11.2528(8)	8.9929(6)
c (Å)	13.2943(5)	23.2818(6)	17.2755(14)	12.1033(8)	13.6094(10)
α (deg)	90	90	90	70.3630(10)	93.7460(10)
β (deg)	118.27	112.23	100.0900(10)	77.1640(10)	95.5470(10)
γ (deg)	90	90	90	88.6080(10)	106.1690(10)
V (Å^3)	4554.5(3)	9691.1(4)	1975.4(3)	1099.54(13)	898.36(11)
Z	8	16	4	2	2
d_{cal} (g/cm^3)	1.493	1.529	1.672	1.525	1.653
μ (mm^{-1})	0.744	0.789	2.820	0.861	3.090
GOF[a] on F^2	1.052	1.057	1.026	1.059	1.018
final R indices	R_1 = 0.0482	R_1 = 0.0460	R_1 = 0.0295	R_1 = 0.0430	R_1 = 0.0353
$[I > 2\sigma(I)]$	wR_2 = 0.1439	wR_2 = 0.1223	wR_2 = 0.0642	wR_2 = 0.1193	wR_2 = 0.0644
R indices[b]	R_1 = 0.0609	R_1 = 0.0703	R_1= 0.0451	R_1 = 0.0545	R_1 = 0.0670
all data[c]	wR_2 = 0.1567	wR_2 = 0.1380	wR_2 = 0.0704	wR_2 = 0.1288	wR_2 = 0.0731

[a] GOF = $[\sum[w(F_o^2 - F_c^2)^2]/(N_o - N_v)]^{1/2}$ (N_o = number of observations, N_v = number of variables). [b] $R_1 = \sum||F_o| - |F_c||/\sum|F_o|$. [c] $wR_2 = [(\sum w(F_o^2 - F_c^2)^2/\sum|F_o|^2)]^{1/2}$.

crystals suitable for X-ray studies. Anal. Calcd. for $C_{21}H_{15}ClMnN_3O_7$: C, 49.28; H, 2.93; N, 8.21. Found: C, 49.26; H, 2.87; N, 8.27. Electronic absorption spectrum in MeCN, λ_{max} (nm) [(ε (M^{-1} cm^{-1})]: 430 (3200), 345 (12 760), 260 (27 330). Selected IR frequencies (KBr disk, cm^{-1}): 2044 (s, ν_{CO}), 1970 (s, ν_{CO}), 1947 (s, ν_{CO}), 1593 (m), 1515 (m), 1374 (w), 1092 (s,ν_{ClO4}), 837 (w), 750 (m), 623 (s), 529 (w). ^{1}H NMR (CD_3CN, 500 MHz), δ (ppm from TMS): 9.00 (s, 1H), 8.82 (dd, 2H), 8.20 (dd, 2H), 8.12 (t, 1H), 7.92 (t, 1H), 7.62 (t, 2H), 7.56 (t, 3H).

$[Mn(qmtpm)(CO)_3(MeCN)]ClO_4$ (2). To a degassed solution of qmtpm (0.153 g, 0.55 mmol) in 25 mL of $CHCl_3$ was added a batch of $[Mn(CO)_3(MeCN)_3]ClO_4$ (0.200 g, 0.55 mmol), and the solution was heated to reflux under N_2 for 6 h. Solvent removal and subsequent trituration with Et_2O afforded **2** as a brick red solid (0.269 g, 88% yield). X-ray quality crystals (red orange plates) were grown by via diffusion of pentane into a CH_2Cl_2 solution of **2**. Anal. Calcd. for $C_{22}H_{17}ClMnN_3O_7S$: C, 47.37; H, 3.07; N, 7.53. Found: C, 47.26; H, 3.10; N, 7.57. Electronic Absorption Spectrum in MeCN, λ_{max} (nm) [ε (M^{-1} cm^{-1})]: 435 (3 680), 335 (10 400), 260 (33 670). Selected IR frequencies (KBr disk, cm^{-1}): 2046 (s, ν_{CO}), 1943 (s, ν_{CO}), 1516 (w), 1438 (w), 1094 (s, ν_{ClO4}), 822 (w), 750 (w), 623 (m). ^{1}H NMR (CD_3CN, 500 MHz), δ (ppm from TMS): 8.97 (s, 1H), 8.82 (t, 2H), 8.20 (t, 2H), 8.12 (t, 1H), 7.91 (t, 1H), 7.55 (d, 1H), 7.49 (t, 1H), 7.38 (t, 1H), 7.27 (s, 1H), 2.52 (s, 3H).

$[Mn(qmtpm)(CO)_3Br]$ (3). A batch of $[Mn(CO)_5Br]$ (0.112 g, 0.41 mmol) was added to a degassed solution of qmtpm (0.113 g, 0.41 mmol) in 20 mL of $CHCl_3$. The solution developed a deep reddish purple hue upon reflux under N_2 atmosphere. After 4 h, the solvent was removed in vacuo, and the residue was triturated three times with Et_2O to obtain a red purple powder (0.219 g, 80% yield). Slow diffusion of pentane into a CH_2Cl_2 solution of **3** afforded red plates suitable for X-ray studies Anal. Calcd. for $C_{20}H_{14}BrMnN_2O_3S$: C, 48.31; H, 2.84; N, 5.63. Found: C, 48.24; H, 2.87; N, 5.52. Electronic Absorption Spectrum in $CHCl_3$, λ_{max} (nm) [ε (M^{-1} cm^{-1})]: 535 (2 235), 335 (9 050), 255 (26 710). Selected IR frequencies (KBr disk, cm^{-1}): 2022 (s, ν_{CO}), 1920 (s, ν_{CO}), 1514 (w), 1434 (w), 1262 (s, ν_{ClO4}), 828 (w), 752 (w), 680 (w).

$[Mn(pmtpm)(CO)_3(MeCN)]ClO_4$ (4). This complex was synthesized by following the procedure that afforded **2** (as described above). A batch of 0.148 g of pmtpm (0.65 mmol) and 0.236 g (0.65 mmol) of $[Mn(CO)_3(MeCN)_3]ClO_4$ afforded 0.269 g (82% yield) of the product as a yellow orange powder. Orange blades suitable for X-ray studies were grown by diffusion of pentane into a CH_2Cl_2 solution of **4**. Anal. Calcd. for $C_{18}H_{12}ClMnN_3O_7S$: C, 42.83; H, 2.40; N, 8.32. Found: C, 42.80; H, 2.46; N, 8.25. Electronic Absorption Spectrum in MeCN, λ_{max} (nm) [ε (M^{-1} cm^{-1})]: 390 (3 620), 270 (17 000). Selected IR frequencies (KBr disk, cm^{-1}): 2042 (s, ν_{CO}), 1945 (s, ν_{CO}), 1592 (w), 1470 (w), 1437 (w), 1307 (w), 1091 (s ν_{ClO4}), 768 (m) 623 (m). ^{1}H NMR (CD_3CN, 500 MHz), δ (ppm from TMS): 9.18 (d, 1H), 8.72 (s, 1H), 8.27 (t, 1H), 8.20 (d, 1H), 7.86 (t, 1H), 7.56 (d, 1H), 7.48 (t, 1H), 7.38 (t, 1H), 7.24 (s, 1H), 2.55 (s, 3H).

$[Mn(pmtpm)(CO)_3Br]$ (5). This complex was synthesized by following the procedure that afforded **3** (as described above). A batch of 0.151 g (0.55 mmol) of $[Mn(CO)_5Br]$ and 0.125 g (0.55 mmol) of pmtpm afforded 0.257 g (47% yield) of **5** as an orange powder. Slow diffusion of pentane into a CH_2Cl_2 solution of **5** afforded red orange plates suitable for X-ray studies. Anal. Calcd. for $C_{16}H_{12}BrMnN_2O_3S$: C, 42.97; H, 2.70; N, 6.26. Found: C, 43.00; H, 2.66; N, 6.20. Electronic Absorption Spectrum in $CHCl_3$, λ_{max} (nm) [ε (M^{-1} cm^{-1})]: 500 (2 530), 380 (2 280), 315 (5 800), 285 (11 260). Selected IR frequencies (KBr disk, cm^{-1}): 2023 (s, ν_{CO}), 1934 (s, ν_{CO}), 1607 (w), 1468 (w), 1303 (w), 775 (w) 680 (w), 627 (w) 514 (w).

Physical Measurements. The ^{1}H NMR spectra were recorded at 298 K on a Varian Unity Inova 500 MHz instrument. A Perkin-Elmer Spectrum-One FT-IR was employed to monitor the FTIR spectra of the compounds. Electronic absorption spectra were obtained with a Varian Cary 50 Spectrophotometer. Room temperature magnetic susceptibility measurements were performed with the aid of a Johnson Matthey magnetic susceptibility balance.

Photolysis Experiments. For continuous wave photolysis experiments, a Newport Oriel Apex Illuminator (150 W xenon lamp) equipped with an Oriel 1/8 m Cornerstone monochromator (measured power 146−150 mW) was used as the light source. Standard ferrioxalate actinometry was performed to calibrate the light source at 509 nm (ϕ_{509}).[30] Samples of **1**−**5** were prepared under dim

dx.doi.org/10.1021/ic3018216 | Inorg. Chem. 2012, 51, 11930−11940

Table 2. Selected bond Distances (Å) and Angles (deg) for 1−5

	1	2	3	4	5
Mn−N1	2.126(2)	2.120(2)	2.106(2)	2.054(2)	2.054(2)
Mn−N2	2.053(2)	2.063(3)	2.059(2)	2.069(2)	2.049(2)
Mn−N3	2.015(2)	2.013(3)		2.019(3)	
Mn−Br			2.5366(6)		2.5338(5)
Mn−C1	1.819(3)	1.810(4)	1.800(4)	1.810(3)	1.802(3)
Mn−C2	1.834(3)	1.831(4)	1.804(3)	1.803(3)	1.806(3)
Mn−C3	1.801(3)	1.803(4)	1.790(4)	1.801(3)	1.781(4)
C1−O1	1.139(3)	1.132(4)	1.149(4)	1.142(4)	1.148(3)
C2−O2	1.131(4)	1.134(4)	1.148(4)	1.150(4)	1.148(3)
C3−O3	1.136(4)	1.145(4)	1.146(4)	1.141(4)	1.148(4)
C1−Mn−N1	171.95(10)	169.99(14)	172.74(12)	173.86(12)	174.35(12)
C2−Mn−N2	175.85(12)	173.15(14)	170.35(12)	172.02(13)	171.15(12)
C3−Mn−N3	177.11(12)	176.07(14)		176.31(11)	
C1−Mn−C2	87.02(12)	86.82(18)	86.11(14)	88.96(16)	89.87(14)
C1−Mn−C3	87.56(14)	91.09(17)	89.42(15)	90.14(15)	88.92(14)
C1−Mn−N2	93.94(10)	91.75(15)	94.18(12)	95.77(12)	97.25(11)
C1−Mn−N3	94.28(11)	91.68(15)		93.41(13)	
C2−Mn−C3	87.51(15)	87.95(18)	89.48(14)	89.17(15)	91.25(14)
C2−Mn−N1	101.03(11)	102.79(14)	101.07(12)	97.05(13)	94.12(12)
C2−Mn−N3	94.80(12)	89.43(14)		89.88(13)	
C3−Mn−N1	92.61(12)	92.62(13)	91.68(12)	88.66(11)	94.98(12)
C3−Mn−N2	88.50(12)	98.73(14)	100.17(12)	97.23(11)	94.14(11)
Mn−C1−O1	177.4(3)	179.9(4)	175.1(3)	177.0(3)	176.9(3)
Mn−C2−O2	174.7(3)	173.8(4)	174.4(3)	177.9(4)	178.6(3)
Mn−C3−O3	177.2(3)	174.6(4)	174.9(3)	177.2(3)	176.0(3)
C1−Mn−Br			91.31(11)		88.55(10)
C2−Mn−Br			84.81(10)		86.97(10)
C3−Mn−Br			174.18(10)		176.91(10)

light conditions and placed in 2 × 10 mm quartz cuvettes positioned 2 cm away from the light source.

Because of differences in solubilities, the quantum yields (ϕ) of CO release for **1**, **2**, and **4** were measured in MeCN (1.10 mM), while that of **3** and **5** were measured in tetrahydrofuran (THF, 1.10 mM). Solutions were prepared to ensure sufficient absorbance (>90%) at the irradiation wavelength (509 nm), and changes in the electronic spectra in the 350−550 nm region (<10% photolysis) were used to determine the extent of CO release. Each sample was irradiated with the monochromatic light (power: 5 mW) at defined time intervals. Changes in the respective charge transfer bands of **1**−**5** were monitored along the 2 mm path.

The apparent rates of photolysis were monitored at an appropriate wavelength for each carbonyl, and the absorbance versus time plots were fitted to a the three parameter exponential equation $A(t) = A_\infty + (A_o - A_\infty)\exp\{-k_{CO}t\}$, where A_o and A_∞ are the initial and final absorbance values, respectively. The apparent rate of CO loss (k_{CO}) was calculated from the $\ln(C)$ versus time (T) plot for each carbonyl.

X-ray Crystallography. Diffraction data for **1**−**5** were collected at 296 K on a Bruker APEX-II instrument using monochromated Mo−K_α radiation (λ = 0.71073 Å). All data were corrected for absorption, and the structures were solved by direct methods using SHELXTL (1995−99) software package (Bruker Analytical X-ray Systems Inc.). Additional refinement details are contained in CIF files (Supporting Information). Crystal data, instrument and data collection parameters are summarized in Table 1. Selected bond distances and angles are listed in Table 2.

DFT and TDDFT Calculations. Density functional theory (DFT) and time dependent density functional theory (TDDFT) studies were executed with PC-GAMESS program[31] using the hybrid functional B3LYP. Optimizations for the Mn atom were performed by employing the LANL2DZ basis set and effective core potential (ECP). The Pople 6-311G* split-valence triple-ζ basis set with polarization was used for Br while for all other atoms, the 6-31G* basis set was employed with Valence Double-ζ polarization (VDZP). The X-ray crystal structure coordinates of complexes (**1**−**5**) were used as a starting point for the gas-phase geometry optimization of the low spin (S = 0) ground states. Electronic transition energies and oscillator strengths were then calculated for **1**−**5** at their B3YLP-optimized geometries using TDDFT. For these calculations the 40 lowest energy electronic excitations were calculated for each compound, and solvent effects were added using the Polarized Continuum Model (PCM)[32] using EtOH and THF as the solvents for the cationic and neutral species, respectively. The calculated molecular orbitals were visualized using MacMolPlt.

RESULTS AND DISCUSSION

To promote CO photorelease from our designed photo-CORMs through metal-to-ligand charge transfer (MLCT) transitions, we have introduced conjugated ring systems in addition to imine functionality in the ligand frames of the present work. Out of the set **1**−**5**, **1** contains the ligand pimq (Figure 1) in which a phenyl ring is bonded to a quinoline donor through an imine linker. This bidentate ligand provides a significant extent of conjugation. The next subset comprising **2** and **4** is derived from the potentially tridentate ligands qmtpm and pmtpm which includes a thioether moiety on the phenyl part of the ligand. The reasons for this inclusion are 2-fold. First, it is expected to add electron density to the π-frame of the ligand and second, it could bind to the Mn(I) center[33] and promote further CO release upon illumination. In addition, a pyridine donor in pmtpm (in complex **4**) has been replaced with a more-conjugated quinoline donor in qmtpm (in complex **2**) for enhanced absorptions in the visible range. Finally, in the subset consisting of **3** and **5**, a Br^- ligand replaces the

dx.doi.org/10.1021/ic3018216 | Inorg. Chem. 2012, 51, 11930−11940

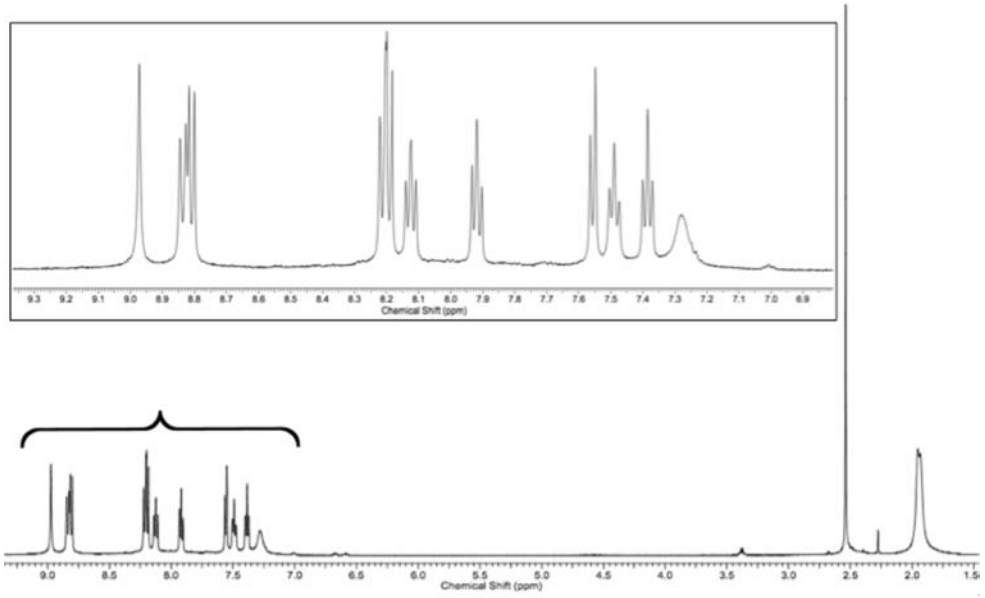

Figure 2. ^{1}H NMR (500 MHz) spectrum of $[Mn(qmtpm)(CO)_3(MeCN)](ClO_4)$ (**2**) in CD_3CN (1.50−9.50 ppm range).

acetonitrile ligand. Introduction of this donor is intended to provide electron density to the Mn(I) center via σ-donation and modulate the MLCT transitions of the resulting carbonyls. In this subset, exchange of the pyridine donor with a quinoline donor has also been applied to correlate the CO photolability of the resulting carbonyls.

Treatment of *fac*-$[Mn(CO)_3(MeCN)]ClO_4$ with pimq or qmtpm in $CHCl_3$ under refluxing conditions afforded the cationic species $[Mn(L)(CO)_3(MeCN)]^+$, where L = pimq (**1**) or qmtpm (**2**). While qmtpm has potentially three coordination sites, only the nitrogen atoms of the ligand were found to bind to the metal center as evidenced by crystallographic data (vide infra). The use of a more suitable starting salt such as $Mn(CO)_5Br$ under similar conditions also did not lead to the desired metal−sulfur binding and instead generated the neutral carbonyl $[Mn(qmtpm)(CO)_3Br]$ (**3**, Figure 4). A similar trend was also observed with the less conjugated ligand pmtpm, wherein reaction with *fac*-$[Mn(CO)_3(MeCN)]ClO_4$ or $Mn(CO)_5Br$ generated compounds **4** and **5**, respectively. This outcome was somewhat surprising since scrutiny of the literature revealed a few low valent manganese carbonyls in which multiple thioether groups are coordinated to the metal center in the presence of π-acceptor ligands.[31] We suspect that the rigid framework of the conjugated ligands of Figure 1 does not allow binding in the *facial* orientation and hence replacement of the MeCN or Br^- ligand was not achieved in **2**−**5**. The utility of the −SMe moiety is however evident in the enhancement of the CO photorelease from these species thus indicating its electronic effect(s) on the overall CO- donating capacity of these photoCORMs (vide infra). All five carbonyls dissolve in organic solvents such as MeCN, DMSO, and $CHCl_3$ and in polar aprotic solvents such as MeOH. Such solutions are stable for hours when kept in the dark.

The IR spectra of carbonyls **1**−**5** exhibit two strong bands in the carbonyl region (Supporting Information), a pattern consistent with known *fac*-Mn(I) tricarbonyl complexes.[34] In the case the MeCN-adducts **1**, **2**, and **4**, the first ν_{CO} stretch appears as a sharp peak at 2042−2044 cm^{-1} pertaining to the axial CO ligand. The second broad ν_{CO} band noted at ∼1942−1947 cm^{-1} features a minor splitting pattern which suggests a distinction between the remaining CO groups in the equatorial plane. For the neutral compounds **3** and **5**, a similar pattern is observed, albeit slight shift to lower frequencies. The first sharp ν_{CO} stretch appears at 2020 cm^{-1} followed by the broad ν_{CO} stretch at 1920−1934 cm^{-1}.

Compounds **1**−**5** are diamagnetic in the solid state and in solutions. The S = 0 state of the compounds is readily evidenced by their clean NMR spectra. An example is shown in Figure 2. In this spectrum of **2** ligation of the qmtpm ligand to the Mn(I) center is indicated by the downfield shift of the imine proton (from 8.73 ppm in the free ligand) to 8.97 ppm. The aromatic protons spread over 7.30−9.00 ppm while the -SMe resonance of qmtpm remains unchanged and appears at 2.52 ppm.

Structures of the Complexes. The structures of the three MeCN-bound cationic carbonyls **1**, **2**, and **4** are discussed first. The cations of these carbonyls all adopt a similar motif wherein the designed ligands pimq (in **1**), qmtpm (in **2**), and pmtpm (in **4**) are coordinated in a bidentate fashion. The structures of **1** and **2** are shown in Figures 3 and 4 respectively while the

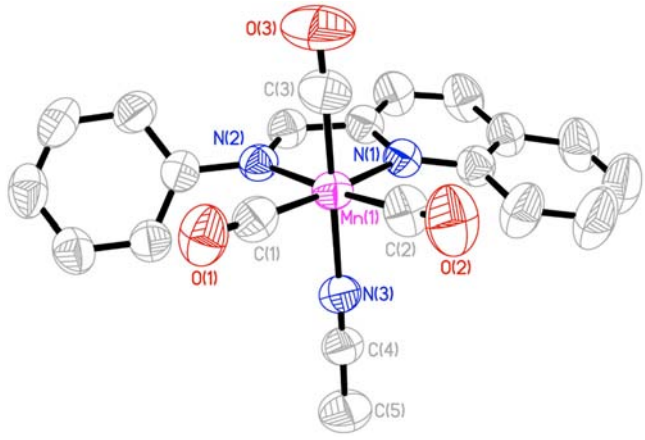

Figure 3. Thermal ellipsoid (probability level 50%) plot of $[Mn(pimq)(CO)_3(MeCN)]^+$ (cation of **1**) with select atom labeling. H atoms have been omitted for clarity.

dx.doi.org/10.1021/ic3018216 | *Inorg. Chem.* 2012, 51, 11930−11940

structure of **4** is included in the Supporting Information, Figure S1. Three facially coordinated CO ligands force the bidentate ligands and MeCN to occupy different planes in the slightly distorted octahedral geometry. The Mn(I)-N_{imine} bond distances of **1** and **2** (2.053(2) and 2.063(3) Å respectively) are similar to such distances noted in other Mn(I) tricarbonyls featuring bidentate diimine ligands.[35] Also, the Mn(I)-$N_{quinoline}$ bond lengths for **1** and **2** (2.126(2) and 2.120(2) Å) compare well with Mn(I) complexes derived from quinoline-containing ligands.[36] These distances are however longer than the Mn(I)-N_{py} bond distance in **4** (2.054(2) Å) and confirm the superior coordinating ability of the pyridine N of the pmtpm ligand. In **2** (and **4**, Supporting Information, Figure S1), the thioether moiety is not coordinated despite the possibility of binding the metal center through displacement of a proximal CO (Figure 4). This presumably arises from the relatively low π-accepting capacity of the thioether S donor compared to CO.

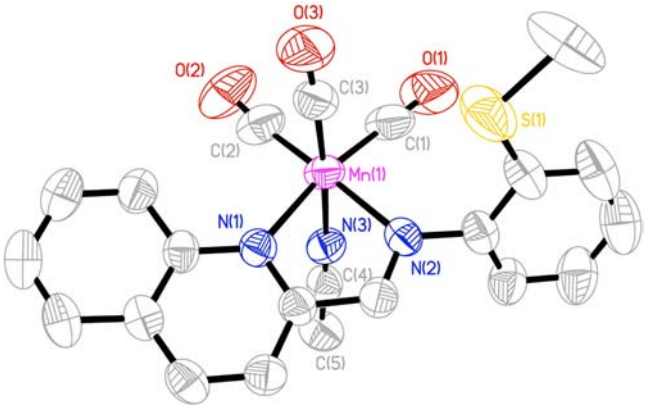

Figure 4. Thermal ellipsoid (probability level 50%) plot of $[Mn(qmtpm)(CO)_3(MeCN)]^+$ (cation of **2**) with select atom labeling. H atoms have been omitted for clarity.

The structure of the neutral carbonyl $[Mn(qmtpm)(CO)_3Br]$ (**3**) (shown in Figure 5) is very similar to that of

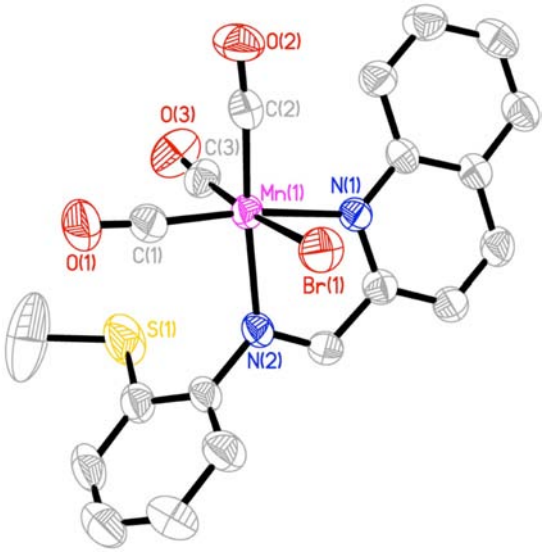

Figure 5. Thermal ellipsoid (probability level 50%) plot of $[Mn(qmtpm)(CO)_3Br]$ (**3**) with select atom labeling. H atoms have been omitted for clarity.

2 except for the replacement of the MeCN ligand with Br^-. The three CO ligands are coordinated in the same facial configuration, and the thioether moiety is not coordinated. In **3**, the Mn(I)-Br distance is 2.5366(6) Å, a value well within the range of Mn(I)-Br distances noted in compounds such as $[BrMn(CO)_2(N,N,N\text{-dapa})]$ [N,N,N-dapa = 2,6-diacetylpyridine-bis(aniline)].[37] The structure of the analogous neutral carbonyl $[Mn(pmtpm)(CO)_3Br]$ (**5**) has been included in the Supporting Information, Figure S2.

Electronic Spectra and CO Release in Solution. The electronic absorption spectra of compounds **1**–**5** have been recorded in MeCN, THF, and $CHCl_3$. A plot of the respective absorption maxima of **2**–**5** (solution in $CHCl_3$) in the visible region is shown in Figure 6. All absorption spectra were

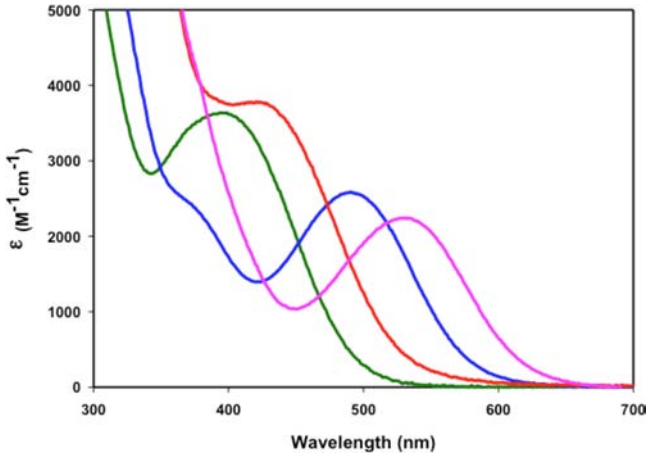

Figure 6. Electronic absorption spectra of $[Mn(qmtpm)(CO)_3(MeCN)]ClO_4$ (**2**, red trace), $[Mn(qmtpm)(CO)_3Br]$ (**3**, pink trace), $[Mn(pmtpm)(CO)_3(MeCN)]ClO_4$ (**4**, green trace), and $[Mn(pmtpm)(CO)_3Br]$ (**5**, blue trace) in $CHCl_3$.

measured in the absence of room light since these carbonyls exhibit facile CO release (vide infra) upon illumination. The effect of increased conjugation in the ligand frame is readily indicated by the *red shift* of the absorption maximum of **2** (435 nm) compared to that of **4** (390 nm). Replacement of the MeCN ligand with the σ-donating Br^- ligand results in *further red shift* of λ_{max} of **3** and **5** to 535 and 500 nm, respectively. Carbonyls **1** and **2** exhibit similar absorption profiles (Supporting Information, Figure S3). with bands centered at ~435, 335, and 265 nm. However, the addition of the −SMe group on the ligand frame leads to moderate increase in the extinction coefficient of **2** compared to **1**.

The high extinction coefficient values for these bands in the 400–600 nm region confirm that they arise from charge transfer transition. Also, the red shift of these bands with more conjugation in the ligand frame (and/or electron-rich ligands or groups in the coordination sphere) readily identifies them as MLCT transition and results of theoretical calculations corroborate this assignment (vide infra).

Although solutions of **1**, **2**, and **4** in MeCN or MeOH are stable for several hours in the dark, exposure of such solutions to low power visible light leads to dramatic changes associated with CO release. Changes in the absorption spectrum of **2** upon illumination with 509 nm monochromatic light (5mW) are shown in Figure 7. Clean isosbestic points 500, 400, and 335 nm confirm that CO loss does not proceed via decomposition. Likewise, THF solutions of **3** and **5** exhibit

dx.doi.org/10.1021/ic3018216 | *Inorg. Chem.* 2012, 51, 11930–11940

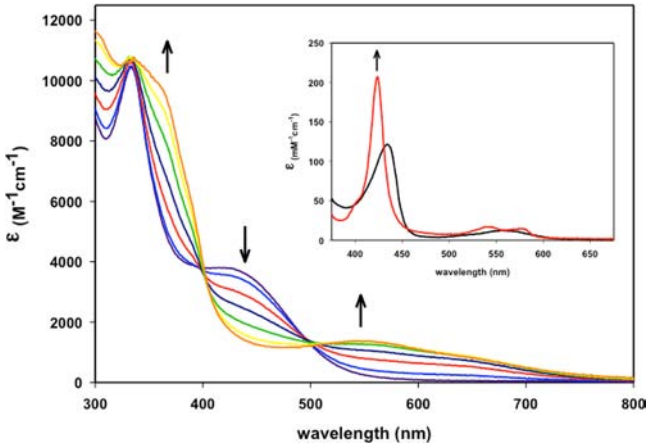

Figure 7. Changes in the electronic absorption spectrum of $[Mn(qmtpm)(CO)_3(MeCN)](ClO_4)$ (**2**) in MeCN upon exposure to monochromatic light (λ = 509 nm, 5mW). Inset: Formation of CO-Mb with light induced CO release from **2** in 100 mM phosphate buffer (pH 7.4).

stability in the dark, and CO release is only triggered upon illumination with 509 nm light with isosbestic points for **3** at 415 and 290 nm (Supporting Information, Figure S4).

Light-induced CO release of compounds **1**−**5** has been investigated by a modified myoglobin assay. In a typical experiment, MeCN or THF solutions of **1**−**5** were degassed and subsequently irradiated with a broadband light source fitted with a 400 nm cutoff filter. The resulting solution was flushed with N_2 gas, and the photogenerated CO was transferred via a cannula into a cuvette containing reduced myoglobin (Mb) in phosphate buffer (pH 7.4). In this method the possibility of carbonyl reduction by dithionite is eliminated.[38] In all cases, shift in the Soret band from 435 to 424 nm confirmed the formation of CO-Mb under anaerobic conditions (Figure 7 Inset). Because CO release takes place only upon light irradiation, it is evident that **1**−**5** comprise *an effective set of Mn-based photoCORMs*. Although the present carbonyls contain three CO ligands, we have not determined the exact number of CO molecules lost from each photoCORM under illumination. Ford and co-workers have commented on this issue in their work with the photoCORM $Na_3[W(CO)_5(TPPTS)]$. Exhaustive photolysis of this carbonyl afforded product(s) that still exhibited CO-related IR bands in its spectrum.[20] In our work, we have also noted that the exact amount of CO release from the photoCORMs upon illumination is quite difficult to quantify because of subsequent secondary reaction(s) of the initial photoproduct(s) with the oxygen, solvent, and other species in solution. Under strict anaerobic conditions, prolonged photolysis of the present carbonyls **1**−**5** in solvents like MeCN and THF afford products that exhibit weak CO stretching frequencies in the 2050−1950 cm^{-1} region. NMR measurements on these products indicated the presence of the intact ligand frames. When the photolysis experiments were performed with solutions in open vials, the final photoproducts exhibited strong EPR signals indicating formation of Mn(II) species. In a recent account, Kurt and Berends have reported the formation of both Mn(II) and Mn(III) species in photolysis of the photoCORM *fac*-$[Mn(CO)_3(tpm)]PF_6$ (tpm = tris(pyrazolyl)methane) under aerobic conditions.[39] Clearly, CO release from CORMs bearing multiple CO ligands follow complicated pathways leading to multiple photoproducts, and hence we have not attempted to characterize the photoproducts from **1**−**5** in the present study .

The CO release capacities of **1**−**5** under illumination with visible light have been determined in the present study to correlate the CO-releasing parameters with the features of the ligand (such as conjugation) and the nature of the sixth ligand (MeCN vs Br^-). For all these carbonyls, the rates of CO release obey a pseudo-first-order behavior (Supporting Information, Figure S4). The apparent rates of CO photorelease (k_{CO}) and the quantum yield values at 509 nm (ϕ_{509}) for **1**−**5** are shown in Table 3. The k_{CO} values of **1**, **2**, and **4** were measured in

Table 3. Apparent Rates of CO Release (k_{CO}) and Associated Quantum Yield Values at 509 nm (ϕ_{509}) of 1−5

compound	apparent rate (s^{-1}) (concentration = 1.10 mM)	quantum yield
1 (solv: MeCN)	$1.4 \times 10^{-3} \pm 0.1$	0.130 ± 0.010
2 (solv: MeCN)	$2.0 \times 10^{-3} \pm 0.1$	0.208 ± 0.010
3 (solv: THF)	$2.6 \times 10^{-3} \pm 0.1$	0.370 ± 0.010
4 (solv: MeCN)	$1.1 \times 10^{-3} \pm 0.1$	0.116 ± 0.010
5 (solv: THF)	$2.1 \times 10^{-3} \pm 0.1$	0.340 ± 0.010

CH_3CN, while those of **3** and **5** were obtained with THF solutions because of differences in solubility. As evident from Table 3, with increased conjugation in the ligand frame (going from **4** to **2**), the k_{CO} value increases from $1.1 \times 10^{-3} \pm 0.1$ to $2.0 \times 10^{-3} \pm 0.1$ s^{-1}. In addition, replacement of MeCN with Br^- (going from **2** to **3**) leads to a significant increase in the k_{CO} value (from $2.0 \times 10^{-3} \pm 0.1$ to $2.6 \times 10^{-3} \pm 0.1$ s^{-1}). The effect(s) of incorporating the −SMe group on the ligand frame is evident in the k_{CO} and ϕ_{509} values of **1** and **2**. The electron-rich S center enhances the ϕ_{509} value of **2** (0.208 ± 0.010) compared to **1** (0.130 ± 0.010) to a noticeable extent. Collectively, these correlations support our previous finding related to increased CO photolability with greater conjugation in the ligand frame.[25] In addition, the present results suggest that the ancillary ligands (like Br^-) can also influence the extent of CO photorelease. Since the −SMe donor is not coordinated to the Mn(I) center in **2**−**5**, it is not immediately evident why such modification of the ligand frames (as shown in Figure 1) affects the CO photolability of these photoCORMs. The results of DFT and TDDFT calculations, as described below, however provide valuable insight into the origins of such enhancement of CO photorelease in **2**−**5** (compared to **1**).

DFT and TDDFT Calculations. DFT and TDDFT calculations were utilized to obtain the optimized geometries, molecular orbital electron densities, and calculated electronic transitions for **1**−**5** to understand how the structural features of these photoCORMs correlate with their capacities of CO photorelease. The DFT optimized structures of **1**−**5** show good agreement with the bond lengths and bond angles observed in the corresponding crystal structure of each complex. Such data for **2**, **3**, and **5** are listed in Table 4 while the rest (for **1** and **4**) are included in Supporting Information, Table S1. The agreement supports the theoretical treatment of the molecules and allowed us to continue on with the TDDFT calculations. The calculated electronic transitions with oscillator strengths above 0.004 were collected, and those with energies falling within the range of the lowest energy experimental absorption band of each complex are presented in Table 5. For

dx.doi.org/10.1021/ic3018216 | *Inorg. Chem.* 2012, 51, 11930−11940

Table 4. Selected Bond Distances (Å) and Angles (deg) of 2, 3, and 5 along with Optimized DFT Bond Distances and Bond Angles for Comparison

	complex **2**		complex **3**		complex **5**	
	X-ray	DFT	X-ray	DFT	X-ray	DFT
Mn−N1	2.120(2)	2.163	2.106(2)	2.166	2.054(2)	2.095
Mn−N2	2.063(3)	2.093	2.059(2)	2.088	2.049(2)	2.071
Mn−N3	2.013(3)	2.045				
Mn−Br			2.536(6)	2.586	2.5338(5)	2.581
Mn−C1	1.810(4)	1.831	1.800(4)	1.820	1.802(3)	1.828
Mn−C2	1.831(4)	1.823	1.804(3)	1.824	1.806(3)	1.820
Mn−C3	1.803(4)	1.852	1.790(4)	1.804	1.781(4)	1.803
C1−Mn−C2	86.82(18)	89.07	86.11(14)	88.12	89.87(14)	91.09
C1−Mn−C3	91.09(17)	97.25	89.42(15)	92.47	88.92(14)	91.69
C1−Mn−N2	91.75(15)	92.05	94.18(12)	93.25	97.25(11)	96.23
C1−Mn−N3	91.68(15)	90.05				
C2−Mn−C3	87.95(18)	96.14	89.48(14)	92.81	91.25(14)	93.07
C2−Mn−N1	102.79(14)	99.21	101.07(12)	100.18	94.12(12)	93.75
C2−Mn−N3	89.43(14)	85.77				
C3−Mn−N1	92.62(13)	84.85	91.68(12)	91.04	94.98(12)	94.45
C3−Mn−N2	98.73(14)	94.14	100.17(12)	100.16	94.14(11)	94.50
C1−Mn−Br			91.31(11)	89.97	88.55(10)	87.40
C2−Mn−Br			84.81(10)	82.30	86.97(10)	85.68

Table 5. Energies (*E*, nm) and Oscillator Strengths (*f*) of the Calculated (TDDFT) Electronic Transitions with the Molecular Orbitals Involved with Each Transition[a]

energy (nm)	oscillator strength (*f*)	transitions
	$[Mn(pimq)(CO)_3(MeCN)]^+$ (**1**)	
431.98	0.0259762	π(Q)-π(Ph)-π(MnCO)→π(Q)-π(SB)[HOMO→LUMO]
406.74	0.0573702	π(Q)-π(Ph)-d_{xz}(Mn)→π(Q)-π(SB)[HOMO-1→LUMO]
388.95	0.0307494	π(MnCO)-π(Ph)→π(Q)-π(SB)[HOMO-2→LUMO]
	$[Mn(qmtpm)(CO)_3(MeCN)]^+$ (**2**)	
533.21	0.0450962	π(PhS) →π(Q)-π(SB)[HOMO→LUMO]
459.29	0.0122483	π(MnCO)-π(Q)→π(Q)-π(SB)[HOMO-1→LUMO]
432.41	0.0189162	π(MnCO)-π(Q)→π(Q)-π(SB)[HOMO-2/HOMO-3→LUMO]
417.86	0.0334093	π(MnCO)-π(Q)→π(Q)-π(SB)[HOMO-2→LUMO]
	$[Mn(qmtpm)(CO)_3Br]$ (**3**)	
520.47	0.0046467	π(PhS)→π(Q)-π(SB)[HOMO→LUMO]
484.31	0.0166749	p(Br)-π(MnCO)→π(Q)-π(SB)[HOMO-1→LUMO]
460.92	0.0533586	p(Br)-π(MnCO)→π(Q)-π(SB)[HOMO-2→LUMO]
	$[Mn(pmtpm)(CO)_3(MeCN)]^+$ (**4**)	
484.60	0.0301023	π(PhS)→π(Pyr)−π(SB)[HOMO→LUMO]
372.72	0.0491039	π(MnCO)→π(Pyr)−π(SB)[HOMO-2→LUMO]
346.30	0.0606618	π(MnCO)-π(PhS)→π(Pyr)−π(SB)[HOMO-4→LUMO]
	$[Mn(pmtpm)(CO)_3Br]$ (**5**)	
491.25	0.0061503	π(PhS)→π(Pyr)-π(SB)[HOMO→LUMO]
446.20	0.0241548	π(MnCO)-p(Br)→π(Pyr)-π(SB)[HOMO-2→LUMO]

[a]Orbitals with greater contributions listed first. Only transitions with energies corresponding to the lowest energy absorption band observed experimentally for each complex are shown.

1, transitions of interest are the HOMO→LUMO (431 nm), HOMO-1→LUMO (406 nm), and HOMO-2→LUMO (388 nm). These correlate to the broad band observed at 430 nm for **1**. In case of **2**, HOMO→LUMO (533 nm), HOMO-1→LUMO (459 nm), combination orbital HOMO-2/HOMO-3→LUMO (432 nm) and HOMO-3→LUMO (417 nm) all fall under the experimental band at 435 nm. Similarly, the theoretical transitions HOMO→LUMO (520 nm), HOMO-1→LUMO (484 nm), HOMO-2→LUMO (460 nm) correlate to the 535 nm band observed experimentally for **3** while the 390 nm experimental band of **4** corresponds to HOMO→LUMO (484 nm), HOMO-2→LUMO (372 nm), and HOMO-4→LUMO (346 nm) transitions. And finally, the experimental band at 500 nm of **5** includes the theoretical transitions HOMO→LUMO (491 nm) and HOMO-2→LUMO (446 nm). Because these calculated transitions fall within the region of wavelengths that was employed to determine the capacity of CO photolability (as described above), we have examined the electron densities of the molecular orbitals that comprise these levels and check whether these transitions do labilize CO ligand(s) from these designed carbonyls. A complete list of transitions can be found in Supporting Information, Table S2.

dx.doi.org/10.1021/ic3018216 | *Inorg. Chem.* 2012, 51, 11930−11940

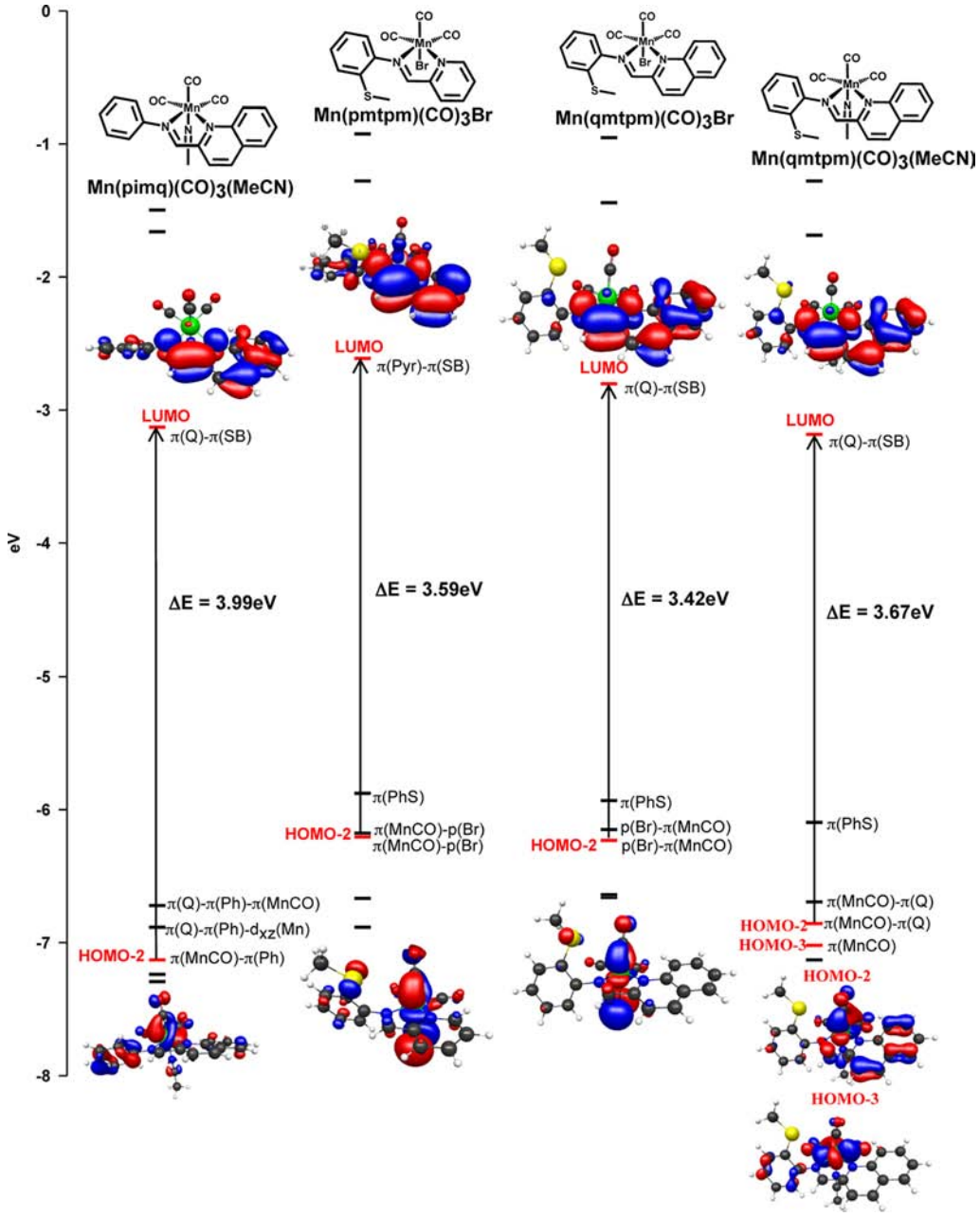

Figure 8. Calculated HOMO/LUMO energy diagram of complexes **1**, **5**, **3**, and **2** (from left to right). The most prominent MOs involved with transitions under the low energy band and their diagrams are shown. Transitions discussed in the text are shown in red (all other orbitals in TDDFT calculations are labeled in black).

The molecular orbital (MO) energy diagram, shown in Figure 8, displays the compositions of the three lowest occupied MOs and the LUMO of **1**, **2**, **3**, and **5**. The first and foremost point to note is that in each photoCORM, the lowest energy band corresponds to transitions that promote electron density from HOMO-2 (predominantly Mn-CO bonding character) to the LUMO mostly composed of the imine functionality and pyridine or quinoline ring. These MLCT transitions therefore shift electron density from the metal center to the ligand π frame, an event that is expected to curb the affinity of the Mn center toward CO (because of loss of π-backdonation from the metal). The CO photolability of the present photoCORMs observed at ~500 nm strongly suggests that these MLCT transitions are responsible for the observed CO photolability. As one goes from **5** to **3**, the change of the pyridine ring to more conjugated quinoline lowers the LUMO level and moves the λ_{max} from 500 to 535 nm. It is therefore evident that enhanced conjugation in the ligand frame sensitizes the resulting photoCORM more to the visible light. Inclusion of the electron-rich Br^- ligand raises both the HOMO-1 and HOMO-2 levels of **3** and **5** (both these MOs include contribution from Br^-, Table 5) compared to the MeCN-bound carbonyls. As a consequence, the MLCT transitions in the visible range are all red-shifted (Figure 8). This finding explains the red shift of these two photoCORMs (535 and 500 nm respectively) compared to **1** (430 nm), **2** (435 nm), and **4** (390 nm).

Although the −SMe group on the ligand frame does not participate in coordination in **2**−**5**, the HOMO of each of these carbonyls is composed of orbitals belonging to the phenyl ring

dx.doi.org/10.1021/ic3018216 | *Inorg. Chem.* 2012, 51, 11930−11940

and the sulfur atom (Figure 8). Thus the HOMO→LUMO transition is an intraligand charge transfer that promotes electron density from the phenyl thioether moiety of the ligand frame to a MO associated mostly with the imine and the corresponding pyridine or quinoline functionality. A close scrutiny of the energy diagram however reveals that the absence of −SMe unit in **1** lowers the energy of the HOMO (consisting mostly of π(Ph) and π(Q) character) and leads to a slight blue shift of the low energy band (430 nm) compared to the analogous carbonyl **2** with −SMe unit on the ligand frame (435 nm). In addition, inclusion of the −SMe unit on the ligand frame enhances both the apparent rate of CO release and the ϕ_{509} value of **2** compared to **1** (Table 3). Since in all the present carbonyls the HOMO→LUMO transition contributes to the low energy band, it appears that the −SMe group enhances the overall CO photolability of **2**−**5** presumably through higher absorption of light in the visible region.

Taken together, the results of the theoretical calculations qualitatively support the hypotheses that guided our design principles. For example, it is evident that low energy MLCT transitions arising from MOs with metal-CO bonding character to MOs associated with the π-frame of the ligand could lead to scission of the Mn-CO bond(s) in the present photoCORMs **1**−**5** upon exposure to visible light. Increase in the CO photolability with more conjugated ligand frames further corroborates this conclusion. Baerends and Rosa have discussed the role of ligand-field and charge-transfer excited states in the photochemical dissociation of metal-CO bonds in metal carbonyls derived from α-diimine ligands.[40] The low energy MLCTs in such carbonyls also play key roles in the CO dissociation pathways. The results of the present work further indicate that inclusion of electron-rich functionality on ligands could enhance the CO photolability. In addition, ancillary ligands such as Br^- significantly augment the sensitivity of the designed photoCORMs (**1**−**5**) toward the visible light. More rigorous theoretical studies to establish the details of the mechanism of CO dissociation arising from the MLCT transition(s) are in progress in this laboratory.

SUMMARY AND CONCLUSIONS

The following are the summary and conclusions of this work.

(1) Five structurally related Mn(I) carbonyls **1**−**5** have been synthesized with a set of Schiff base ligands that contain pyridine and quinoline donors. The extent of conjugation has been systematically varied in these ligand frames. In addition, the effects of an electron-rich −SMe group on the ligand frame and an ancillary Br^- ligand in the coordination sphere have also been examined.

(2) The structures of the carbonyls indicate that the −SMe group does not bind the Mn(I) center in the equatorial plane because of its inability to replace a bound CO ligand. In addition to three facially ligated CO ligands, a MeCN or Br^- is also present.

(3) Although stable in the dark, solutions of all five carbonyls (in MeCN, MeOH, THF, or $CHCl_3$) rapidly release CO upon exposure to low power (5−15 mW) visible light (400−550 nm). These designed carbonyls could therefore be used as photoCORMs. The apparent rates of CO photorelease and quantum yield values at 509 nm (ϕ_{509}) increase linearly with increase in conjugation in the ligand frame. Replacement of MeCN with Br^- causes a significant red shift of the low energy band. Inclusion of the −SMe group on the ligand frame enhances both the apparent rate of CO release and the ϕ_{509} value.

(4) Results of density functional theory (DFT) and time dependent DFT (TDDFT) studies support the design principle that "transfer of electron density from the Mn(I) center to π orbitals of the ligand frame through MLCT transitions could curb the affinity of the metal center toward CO (requiring strong back bonding)". The calculated MO energy diagram also display proper alterations in the energy of the HOMO and LUMO levels upon inclusion of −SMe group and the Br^- ligand that lead to enhanced CO photolability of the respective photoCORMs.

(5) The excellent CO-releasing capacities of **1**−**5** and their sensitivity to visible light strongly support the design principles employed in the present work and provide further incentive toward isolation of new photoCORMs with predictable properties.

ASSOCIATED CONTENT

Supporting Information

X-ray crystallographic data (in CIF format) for $[Mn(pimq)(CO)_3(MeCN)]ClO_4$ (**1**), $[Mn(qmtpm)(CO)_3(MeCN)]ClO_4$ (**2**), $[Mn(qmtpm)(CO)_3Br]$ (**3**), $[Mn(pmtpm)(CO)_3(MeCN)]ClO_4$ (**4**), and $[Mn(pmtpm)(CO)_3Br]$ (**5**), thermal ellipsoid (probability level 50%) plots of **4** (Figure S1) and **5** (Figure S2), absorption profiles of **1** and **2** in MeCN (Figure S3), pseudo-first order plot of ln[**3**] vs time in THF (Figure S4), selected bond distances and angles of **1** and **4** with optimized DFT bond distances and angles (Table S1), complete list of energy and oscillator strength of the calculated (TDDFT) electronic transitions with the involved molecular orbitals (Table S2). This material is available free of charge via the Internet at http://pubs.acs.org.

AUTHOR INFORMATION

Corresponding Author

*E-mail: pradip@ucsc.edu.

Notes

The authors declare no competing financial interest.

ACKNOWLEDGMENTS

This research was supported by the NSF Grant CHE-0957251. M.G. was supported by the IMSD Grant GM-58903 and the NHGRI Grant HG002371. The X-ray facility at UCSC is supported by a NSF Major Research Instrumentation (MRI) Grant (CHE-0521569).

REFERENCES

(1) Kim, H. P.; Ryter, S. W.; Choi, A. M. K. *Pharmacol. Toxicol.* **2006**, *46*, 411−449.

(2) (a) Jaggar, J. H.; Li, A.; Parfenova, H.; Liu, J.; Umstot, E. S.; Dopico, A. M.; Leffler, C. W. *Circ. Res.* **2005**, *97*, 805−812. (b) Ndisang, J. F.; Tabien, H. E. N.; Wang, R. *J. Hypertens.* **2004**, *22*, 1057−1074. (c) Zhang, F.; Kaide, J.; Rodriguez-Mulero, F.; Abraham, N. G.; Nasjletti, A. *Am. J. Hypertens.* **2001**, *14*, 62S−67S. (d) McLaughlin, B. E.; Chretien, M. L.; Choi, C.; Brien, J. F.; Nakatsu, K.; Marks, G. S. *Can. J. Physiol. Pharmacol.* **2000**, *78*, 343−349. (e) Wang, R. *Can. J. Physiol. Pharmacol.* **1998**, *76*, 1−15. (f) Wang, R.; Wu, L.; Wang, Z. *Eur. J. Physiol.* **1997**, *434*, 285−291.

(3) (a) Kim, H. P.; Ryter, S. W.; Choi, A. M. K. *Annu. Rev. Pharmacol. Toxicol.* **2006**, *46*, 411−449. (b) Boczkowski, J.; Poderoso, J. J.; Motterlini, R. *Trends Biochem. Sci.* **2006**, *31*, 614−621. (c) Morse, D.; Sethi, J.; Choi, A. M. K. *Crit. Care Med.* **2002**, *30*, S12−S16.

(4) (a) Ahanger, A. A.; Prawez, S.; Leo, M. D. M.; Kathirvel, K.; Kumar, D.; Tandan, S. K.; Malik, J. K. *Eur. J. Pharmacol.* **2010**, *645*, 165−170. (b) Vieira, H. L. A.; Queiroga, C. S. F.; Alves, P. M. *J. Neurochem.* **2008**, *107*, 375−384. (c) Brouard, S.; Otterbein, L. E.; Anrather, J.; Tobiasch, E.; Bach, F. H.; Choi, A. M.; Soares, M. P. *J. Exp. Med.* **2000**, *192*, 1015−1026.
(5) Zuckerbraun, B. S.; Chin, B. Y.; Bilban, M.; de Costa d'Avila, J.; Rao, J.; Billiar, T. R.; Otterbein, L. E. *FASEB J.* **2007**, *21*, 1099−1106.
(6) Otterbein, L. E.; Bach, F. H.; Alam, J.; Soares, M.; Lu, H. T.; Wysk, M.; Davis, R. J.; Flavell, R. A.; Choi, A. M. K. *Nat. Med.* **2000**, *6*, 422−428.
(7) Kohmoto, J.; Nakao, A.; Stolz, D. B.; Kaizu, T.; Tsung, A.; Ikeda, A.; Shimizu, H.; Takahashi, T.; Tomiyama, K.; Sugimoto, R.; Choi, A. M. K.; Billiar, T. R.; Murase, N.; McCurry, K. R. *Am. J. Transplant.* **2007**, *7*, 2279−2290.
(8) Nakao, A.; Choi, A. M. K.; Murase, N. *J. Cell. Mol. Med.* **2006**, *10*, 650−671.
(9) (a) Ghosh, S.; Wilson, M. R.; Choudhury, S.; Yamamoto, H.; Goddard, M. E.; Falusi, B.; Marczin, N.; Takata, M. *Am. J. Physiol. Lung Cell Mol. Physiol.* **2005**, *288*, L1003−L1009. (b) Fujita, T.; Toda, K.; Karimova, A.; Yan, S. F.; Naka, Y.; Yet, S. F.; Pinsky, D. J. *Nat. Med.* **2001**, *7*, 598−604.
(10) (a) Stein, A. B.; Bolli, R.; Dawn, B.; Sanganalmath, S. K.; Zhu, Y.; Wang, O. L.; Guo, Y.; Motterlini, R.; Xuan, Y. T. *J. Mol. Cell. Cardiol.* **2012**, *52*, 228−236. (b) Stein, A. B.; Guo, Y.; Tan, W.; Wu, W. J.; Zhu, X.; Li, Q.; Luo, C.; Dawn, B.; Johnson, T. R.; Motterlini, R.; Bolli, R. *J. Mol. Cell. Cardiol.* **2005**, *38*, 127−134.
(11) (a) Romão, C. C.; Blättler, W. A.; Seixas, J. D.; Bernardes, G. J. L. *Chem. Soc. Rev.* **2012**, *41*, 3571−3583. (b) Alberto, R.; Motterlini, R. *Dalton Trans.* **2007**, 1651−1660. (c) Johnson, T. R.; Mann, B. E.; Clark, J. E.; Foresti, R.; Green, C. J.; Motterlini, R. *Angew. Chem., Int. Ed.* **2003**, *42*, 3722−3729.
(12) Johnson, T. R.; Mann, B. E.; Teasdale, I. P.; Adams, H.; Foresti, R.; Green, C. J.; Motterlini, R. *Dalton Trans.* **2007**, 1500−1508.
(13) Zhang, W. Q.; Whitwood, A. C.; Fairlamb, I. J. S.; Lynam, J. M. *Inorg. Chem.* **2010**, *49*, 8941−8952.
(14) Fairlamb, I. J. S.; Lynam, J. M.; Moulton, B. E.; Taylor, I. E.; Duhme-Klair, A. K.; Sawle, P.; Motterlini, R. *Dalton Trans.* **2007**, 3603−3605.
(15) Zobi, F.; Blacque, O.; Jacobs, R. A.; Schaub, M. C.; Bogdanova, A. Y. *Dalton Trans.* **2012**, *41*, 370−378.
(16) Bikiel, D. E.; González Solveyra, E.; Di Salvo, F.; Milagre, H. M. S.; Eberlin, M. N.; Corrêa, R. S.; Ellena, J.; Estrin, D. A.; Doctorovich, F. *Inorg. Chem.* **2011**, *50*, 2334−2345.
(17) Gonzalez, M. A.; Fry, N. L.; Burt, R.; Davda, R.; Hobbs, A. J.; Mascharak, P. K. *Inorg. Chem.* **2011**, *50*, 3127−3134.
(18) Herrick, R. S.; Brown, T. L. *Inorg. Chem.* **1984**, *23*, 4550−4553.
(19) Engelking, P. C.; Lineberger, W. C. *J. Am. Chem. Soc.* **1979**, *101*, 5569−5573.
(20) Rimmer, R. D.; Richter, H.; Ford, P. C. *Inorg. Chem.* **2010**, *49*, 1180−1185.
(21) Jackson, C. S.; Schmitt, S.; Dou, Q. P.; Kodanko, J. J. *Inorg. Chem.* **2011**, *50*, 5336−5338.
(22) Kretschmer, R.; Gessner, G.; Görls, H.; Heinemann, S. H.; Westerhausen, M. *J. Inorg. Biochem.* **2011**, *105*, 6−9.
(23) Crook, S. H.; Mann, B. E.; Meijer, A. J. H. M.; Adams, H.; Sawle, P.; Scapens, D.; Motterlini, R. *Dalton Trans.* **2011**, *40*, 4230−4235.
(24) (a) Pfeiffer, H.; Rojas, A.; Niesel, J.; Schatzschneider, U. *Dalton Trans.* **2009**, 4292−4298. (b) Kunz, P. C.; Huber, W.; Rojas, A.; Schatzschneider, U.; Spingler, B. *Eur. J. Inorg. Chem.* **2009**, 5358−5366.
(25) Gonzalez, M. A.; Yim, M. A.; Cheng, S.; Moyes, A.; Hobbs, A. J.; Mascharak, P. K. *Inorg. Chem.* **2012**, *51*, 601−608.
(26) Roy, S.; Mitra, P.; Patra, A. K. *Inorg. Chim. Acta* **2011**, *370*, 247−253.
(27) Castro, A. G.; Costa, J. S.; Pievo, R.; Massera, C.; Mutikainen, I.; Turpeinen, U.; Gamez, P.; Reedijk, J. *Z. Anorg. Allg. Chem.* **2008**, *634*, 2477−2482.
(28) Edwards, D. A.; Marshalsea, J. *J. Orgamomet. Chem.* **1977**, *131*, 73−91.
(29) Hamer, F. M. *J. Chem. Soc.* **1952**, 3197−3211.
(30) Montalti, M.; Credi, A.; Prodi, L.; Gandolfi, M. T. *Handbook of Photochemistry*, 3rd ed.; CRC Press: Boca Raton, FL, 2006.
(31) Nemukhin, A. V.; Grigorenko, B. L.; Granovsky, A. A. *Moscow Univ. Chem. Bull.* **2004**, *45*, 75−102.
(32) Miertus, S.; Scrocco, E.; Tomasi, J. *Chem. Phys.* **1981**, *55*, 117−120.
(33) (a) Patel, B.; Reid, G. *J. Chem. Soc., Dalton Trans.* **2000**, 1303−1307. (b) Connolly, J.; Genge, A. R. J.; Levason, W.; Orchard, S. D.; Pope, S. J. A.; Reid, G. *J. Chem. Soc., Dalton Trans.* **1999**, 2343−2351. (c) Connolly, J.; Goodban, G. W.; Reid, G.; Slawin, A. M. Z. *J. Chem. Soc., Dalton Trans.* **1998**, 2225−2231.
(34) (a) Kunz, P. C.; Huber, W.; Rojas, A.; Schatzschneider, U.; Spingler, B. *Eur. J. Inorg, Chem.* **2009**, 5358−5366. (b) Carlos, R. M.; Carlos, I. A.; Lima Neto, B. S.; Neumann, M. G. *Inorg. Chim. Acta* **2000**, *299*, 231−237. (c) Reger, D. L.; Grattan, T. C.; Brown, K. J.; Little, C. A.; Lamba, J. J. S.; Rheingold, A. L.; Sommer, R. D. *J. Organomet. Chem.* **2000**, *607*, 120−128. (d) Hyams, I. J.; Bailey, R. T.; Lippincott, E. R. *Spectrochim. Acta* **1967**, *23A*, 273−284.
(35) (a) García-Escudero, L. A.; Miguel, D.; Turiel, J. A. *J. Organomet. Chem.* **2006**, *691*, 3434−3444. (b) Valín, M. L.; Moreiras, D.; Solans, X.; Font-Altaba, M.; García-Alonso, F. J. *Acta Crystallogr., Sect. C* **1986**, *42*, 417−418.
(36) Zhang, J. A.; Pan, M.; Jiang, J. J.; She, Z. G.; Fan, Z. J.; Su, C. Y. *Inorg. Chim. Acta* **2011**, *374*, 269−277.
(37) Stor, G. J.; van der Vis, M.; Stufkens, D. J.; Oskam, A. *J. Organomet. Chem.* **1994**, *482*, 15−29.
(38) McLean, S.; Mann, B. E.; Poole, R. K. *Anal. Biochem.* **2012**, *427*, 36−40.
(39) Berends, H.-M.; Kurz, P. *Inorg. Chim. Acta* **2012**, *380*, 141−147.
(40) Baerends, E. J.; Rosa, A. *Coord. Chem. Rev.* **1998**, *177*, 97−125.